Diagenetic priming of submarine landslides in ooze-rich substrates

Nan Wu[1*], Christopher A-L. Jackson[2], Michael A. Clare[3], David M. Hodgson[4], Harya D. Nugraha[5], Michael J. Steventon[6], Guangfa Zhong[1]

[1]State Key Laboratory of Marine Geology, Tongji University, 1239 Siping Road, Shanghai, 200092, China

[2] Department of Earth Science & Engineering, Imperial College, Prince Consort Road, London, SW7 2BP, UK

[3]Ocean BioGeosciences, National Oceanography Centre, Southampton SO14 3ZH, UK

[4]School of Earth and Environment, University of Leeds, Leeds, LS2 9JT, UK

[5]Center for Sustainable Geoscience, Universitas Pertamina, Jakarta, 12220, Indonesia

[6]Shell Research, Shell Centre, London, SE1 7NA, UK

*nanwu@tongji.edu.cn

Abstract

Oozes are the most widespread deep-sea sediment in the global ocean, but very little is known about how changes in their physical properties during burial impact slope stability and related geohazards. Here, we use 3D seismic reflection, geochemical, and petrophysical data acquired both within and adjacent to 13 large (in total c. 6330 km^2) submarine slides on the Exmouth Plateau, NW Shelf, Australia, to investigate how the pre-slide physical properties of oozes control slope failure and emplacement processes. Our integrated dataset allows potential slide surfaces to be detected within ooze successions; a crucial advance for improved submarine geohazard assessment. Moreover, we demonstrate that the interplay of tectonics, ocean current activity, and silica diagenesis can prime multiple slides on very low gradient slopes in tropical, oceanic basins. Therefore, the diagenetic state of silica-rich sediments must be considered to improve slope stability assessments.

Keywords: Submarine landslides; Diagenesis; Oozes

Introduction

Submarine landslides (slides) can trigger tsunami and threaten coastal communities, and damage economically critically seabed infrastructure (e.g., Carter et al., 2012; Clare et al., 2014; Talling et al., 2014). Post-depositional processes can prime substrates to fail, and that instantaneous triggers, such as earthquakes, are not prerequisites for slide initiation (Masson et al., 2010; Talling et al., 2014; Urlaub et al., 2018). Such preconditioning appears to be particularly significant for calcareous oozes, with the biogenic constituents that dominate oozes being highly compressible, water-rich, and prone to brittle inter-particle cementation meaning they have distinct geotechnical properties and failure behaviour (Shiwakoti et al., 2002; Tanaka and Locat, 1999). During burial, these properties mean calcareous oozes are prone to excess pore pressure build up, which causes further strength reduction that can ultimately prime the sediment to fail (Tanaka and Locat, 1999). This could explain why large slides occur on unusually low-angle slopes (<2^{o}) in areas of low sediment accumulation (<0.15 m/kyr) (e.g. Gatter et al., 2021; Urlaub et al., 2018). Despite their apparent significance, the pre-failure physical properties of ooze-rich slopes that ultimately fail remain poorly constrained (Urlaub et al., 2018), given: (i) difficulties in directly sampling and geophysically imaging the base of thick (100s m) slides; and (ii) emplacement processes modify the physical properties of the slope sediment.

Identifying potential failure or shear surfaces within sedimentary sequences is crucial for forecasting future events and modelling landslide motion (Locat et al., 2014). Previous studies have mostly focused on individual slides, originating in diatomaceous, rather than calcareous, oozes. Typically, sampling has been from landslide debris; hence, any geotechnically-weak layers are unlikely to be preserved (Gatter et al., 2021; Locat et al., 2014; Urlaub et al., 2018). Therefore, the pre-emplacement physical properties of sediments at basal shear surfaces remain poorly understood, given they can be strongly modified as the slide evolves (Masson et al., 2010). An understanding of the processes and timescales for priming calcareous ooze-rich slides is crucial to improve geohazard assessments, particularly as calcareous oozes constitute more than 50% of deep ocean floor sediments (Dutkiewicz et al., 2020).

Here we integrate six time-migrated 3D seismic reflection datasets (16,189 km^2; see Appendix S1 for details), a regional network of 2D seismic reflection profiles, and lithological, petrophysical, and geochemical data from Ocean Drilling Program (ODP) Site 762 on the Exmouth Plateau, NW Shelf, Australia (Figure 1A) to answer: i) what are the physical properties of calcareous ooze, and can they explain the stratigraphic occurrence of the basal shear surfaces of large slides? ii) to what extent does silica diagenesis modify subsurface physical properties, and prime substrate for sliding? and iii) how important are regional tectonic and oceanographic controls in the preconditioning of calcareous-ooze slides?

Setting and Methods

Seismic reflection data image 13 slides that cumulatively cover c. 6330 km2 within the Upper Miocene and Recent interval of the Exmouth Plateau (H2 to the seabed; Figure 1B), which is equivalent to Seismic Unit 3 of Nugraha et al. (2018). Industry and ODP 762 boreholes indicate this interval comprises calcareous oozes (Nugraha et al., 2018). ODP 762 is unaffected by sliding, but intersects an interval stratigraphically-equivalent to that hosting the slides, hence we are able to characterize the pre-failure stratigraphy (Figure 2A, 2B). We mapped three age-constrained seismic horizons (H1-3) that define distinct changes in seismic facies and thus bound two seismic units (SU1-2): (i) H1 – intra-Upper Eocene; (ii) H2 – the Late Miocene Unconformity; and (iii) H3 – an undated horizon that defines the top surface of the largest slide (Slide-1; 2,800 km2), which merges with H2 near the Exmouth Plateau Arch (Figure 1C). Variance attributes (see Appendix S2 for explanation) were generated to determine the extent and geometry of the depositional bodies. Seismic reflection data were tied to ODP 762 (see Appendix S3 for details), allowing us to corelate seismic character and sediment properties. Velocity and density data from ODP 762 provide a proxy record of sediment overpressure (Tingay et al., 2009), whereas water content and void ratio are used as proxies for sediment shear strength and compressibility (Gatter et al., 2020; Tanaka and Locat, 1999).

Results

H1: Opal A-CT Conversion Boundary

H1 defines the base of SU1 (Figure 1C), and is offset by numerous, low-throw (<20 ms TWT) polygonal faults that terminate at, or just below, H2 (Figure 1B, 2C). Well-log data reveal a distinct change in petrophysical properties downwards across H1, defined by a sharp increase in bulk density (from 1.80 g/cm^3 to 2.17 g/cm^3) and velocity (from 1.62 km/s to 1.86 km/s), and a decrease in porosity (from 58.0% to 42.5%) and water content (from 30.0% to 20.7%) (Figure 1B). This dramatic downward change in physical properties is expressed in the seismic reflection data by a discrete, c. 40 ms TWT-thick, package of high-amplitude reflections, broadly defined at its top by a positive polarity event (i.e., a downward increase in acoustic impedance; Figure 1B, 2C). X-ray diffraction measurements from ODP 762 also show that sediments above H1 have high concentrations of opal A, whereas below H1, the sediment has high concentrations of opal CT (Figure 1B). H1 therefore corresponds to the opal A-CT conversion boundary (Haq et al., 1990; Nähr et al., 1998).

SU1 - Lower Eocene to Upper Miocene chalk affected by silica diagenesis

The basal part of SU1 is enriched in clinoptilolite (Figure 1B), one of the most common authigenic silicate minerals in pelagic sediments (Nähr et al., 1998). SU1 transitions upwards from competent, hard chalk (Lower Eocene-Upper Eocene) to calcareous ooze (Upper Eocene-Middle Miocene) (Figure 1B), and it is deformed by the polygonal fault system offsetting H1 (Figure 2C). Data from ODP 762 show that the dissolved SiO_2 content increases over a 50 m-thick interval near the top of SU1 (Figure 1B). The dominant diagenetic process associated with SU1 is therefore interpreted to be silica diagenesis, with the locally abundant clinoptilolite interpreted to be caused by the conversion of opal A to CT (Volpi et al., 2003).

H2 – Late Miocene Unconformity and regional failure plane for slides

H2 is a seismically defined reflection that marks the base of SU2 (Figure 2C and Appendix S4 for Slides 2-13). The bases of all 13 slides identified in this unit are on, or only 15-30 m above, H2. Well-log data from ODP 762 indicate H2 corresponds to a major, biostratigraphically-defined unconformity, separating Late Eocene and Late Miocene deposits (Haq et al., 1990; Nugraha et al., 2018). H2 defines a sharp upward increase in terrigenous particles (e.g. quartz, feldspar, and clay), and nearshore coccolithophores (e.g. *Braarudosphaera Bigelow*), the latter being extremely unusual for deep-marine basinal sediments, and providing possible evidence for an abrupt change in the paleo-ocean current regime associated with Australia-Eurasia collision during the Late Miocene (Haq et al., 1990).

Well-log data reveals H2 defines a c. 13 m thick zone with bulk density increasing downward from 1.60 g/cm^3 to 1.85 g/cm^3, and porosity decreasing downward from 80% to 58.5% (Figure 1B, 4E). Although we lack direct measurements of permeability, the localised low porosity and high density responses within H2 may indicate this unit is over-compacted, with a relatively low permeability compared to the surrounding sediment (Sawyer et al., 2009). Conversely, the localised low density and velocity, and high porosity responses below H2 may indicate that abnormally high pore pressures have been trapped below this horizon (Figure 1B; Dugan and Sheahan, 2012; Tingay et al., 2009). It is these sharp changes in petrophysical properties that result in H2 being expressed by a high-amplitude, negative polarity seismic reflection (Figure 1B). Another petrophysically-distinct interval, Hs (c. 5 m thick) can only be revealed from the well data and is recognized immediately above H2 (Figure 1B, 4E). Hs is characterized by an upward decrease in Vp from 1.7 km/s and 1.52 km/s, and an increase in water content from 30.0% to 48.5% (Figure 1B). The extremely low velocity response at the level of Hs indicates possible underpressure at this horizon, whereas the high-water content response indicates Hs has higher compressibility and lower shear strength (Gatter et al., 2020). Nonetheless, direct measurements are needed to achieve a more accurate analysis of the sediment stability that using proxy measures from well data, which will improve future hazard assessments (see also Appendix S5).

SU2: Slide-prone calcareous ooze interval affected by polygonal faulting and dewatering

SU2 contains pure calcareous ooze (Late Miocene-present) (Figure 1B) and is dominated by variable-amplitude, discontinuous reflections, containing moderately deformed package of more continuous, moderate-to-high amplitude reflections. The exception to this being near ODP 762, where continuous, low-amplitude reflections occur (Figure 1C). We interpret that the discontinuous and continuous seismic facies represent slide (e.g., Bull et al., 2009) and background slope deposits, respectively. We now focus on Slide-1, the largest and best-imaged slide, to investigate the role of substrate preconditioning and triggering of the slides (Figure 2A, 2B).

Below Slide-1, H1 is crosscut by numerous polygonal faults that tip-out upward at or near its basal shear surface (i.e., H2; Figure 3A, 3B). H3 defines the top of Slide-1 and is a medium-amplitude reflection (Figure 3A). Directly beneath H2 are numerous high-amplitude, concave reflections that are developed close to the upper termination of the faults (Figure 3A). In planform, these reflections define sub-circular (<100 m in diameter) to elliptical (100-500 m long-axis length) depressions (Figure 3C), interpreted as localised accumulation of fluid or gas (e.g. Paganoni et al., 2019). The high-amplitude concave reflections resemble zones of fluid expulsion or gas migration as observed elsewhere on the Exmouth Plateau (Foschi and Cartwright, 2020; Paganoni et al., 2019).

Discussion and Conclusion

Controls on the formation of a regional failure surface and slide emplacement

Compared with H2, the 5 m-thick Hs is characterized by relatively high-water content and void ratio (and hence low shear strength and high compressibility) and a low acoustic velocity, both indicative of overpressure (Figure 4E). The geotechnical contrast between impermeable strata above H2 and the overlying water-saturated, over-pressured ooze of SU2, created a weak layer (Hs), providing ideal conditions for slope failure, even on very low angle slopes. We propose this explanation for why all thirteen slides share a stratigraphically-equivalent failure surface, with Hs ultimately being locally entrained by the slides.

A similar diagnosis was made in the shallower water Finneidfjord, Norway, where multiple, asynchronous fjord-flank slides share a regional failure plane, above which a low density, over-pressured layer was deposited (L'Heureux et al., 2012). While the source of the weak layer was terrestrially-derived mud and not deep water calcareous ooze, the similarity of a highly compressible fluid-charged mud overlying an impermeable basal layer is striking. Overpressure in Finneidfjord is related to the infiltration of meteoric groundwater. However, such terrestrially-linked charging is not possible in the deep water setting of the Exmouth Plateau, thus we discuss alternative mechanisms for overpressure development and subsequent slope failure. *Silica diagenesis as a primer for slope instability and failure, and slide emplacement*

We suggest that the most likely source for overpressure relates to the generation and release of fluids during silica diagenesis, which is a well-known dehydration reaction (e.g., Davies et al., 2009; Volpi et al., 2003). Silica diagenesis occurs after the calcareous ooze overburden was presented in SU2, followed by fluid expulsion and polygonal faults generation (Figure 4A-C and Appendix S6). The pronounced downward decrease in porosity and water content below H1 suggests a large amount of fluid was expelled from the opal A-CT conversion zone (Figure 4C; Davies and Clark, 2006). This fluid migrated upward, likely along polygonal faults (e.g. Davies et al., 2009; Gay et al., 2006) and became trapped beneath the lower permeability H2, forming stratigraphically-controlled overpressure and lowering the sediment shear strength (Figure 4C&D). Whether such fluid migration is steady and continuous, or intermittent, perhaps triggered by transient periods of seismicity, is unclear (e.g. Embriaco et al., 2014). The continuous overburden from calcareous oozes could also lead to excess pore pressure and ultimately destabilize a low gradient slope (Tanaka and Locat, 1999). Moreover, it is plausible that enhanced seismicity, as a result of the Australian and Eurasian plates colliding during the Early Miocene, triggered fluid flow and even slope failure (Nugraha et al., 2018). Regardless, our findings support silica diagenesis priming submarine slope instability and the emplacement of a slide (c. 110 km^2 in area), which is a mechanistic control proposed for slides in other slope successions (Davies and Clark, 2006; Volpi et al., 2003). Our study is the first to show that silica diagenesis can form a regional failure plane for multiple, large volume submarine landslides, and to identify this control in a tropical setting. *Role of tectonics and paleo-oceanography in priming and dictating the location of slope failure*

During the Late Miocene, the collision of the Australia and Eurasia Plates caused the Indonesian ocean gateway to narrow offshore north Australia (Nugraha et al., 2018). This increased the strength of the southward-flowing Leeuwin Current and suppressing the deep northward-flowing Western Australia Current (Rai and Singh, 2001). These tectonically-driven variations fundamentally controlled the benthic and planktonic foraminiferal assemblages (Kennett, 1985), and hence the abrupt contrast in lithology and physical properties at H2 that subsequently primed slides failure depth and location. The interplay of multiple physical processes on slide preconditioning can be felt thousands, or even millions, of years after their activity ceased (Gatter et al., 2020), thus cautioning against the simplistic linkage of sliding to an external trigger. We suggest that such a temporally-buffered connection likely exists for many other settings, where diverse tectonic, sedimentological and/or oceanographic process interactions form stratigraphically-constrained fluid sources, pathways, and permeability barriers (Gatter et al., 2021; Gatter et al., 2020).

Figure Caption

Figure 1. (A) Location of the study area. The red polygons and grey lines represent the 3D and 2D seismic reflection data, respectively. (B) Log-seismic integration at ODP 762. (C) Regional composite seismic section showing the main tectonic elements and seismic units.

Figure 2. (A) Time structure map, which shows the location of the thirteen slides that have shaped the seabed of the study area. (B) Sketch of Figure 2A. (C) Seismic reflection section across Slide-1 showing the key seismic horizons (H1-3) and seismic units (SU1&2).

Figure 3. (A) Zoomed-in seismic section of Slide-1. (B) Variance time slice calculated at c. 130 ms below Slide-1, revealing polygonal fault systems. (C) Variance time slice calculated at c.

40 ms below Slide-1, showing sediments accumulation structures. See the location of Figure 3 in Figure 2B.

Figure 4. Schematic diagram showing the development of the slides. (A) Deposition of the siliceous chalk stage. (B) Deposition of the calcareous ooze and opal A-CT conversion stage. (C) Polygonal faults, fluid migration, and excess pore pressure generation stage. (D) Emplacement of the regionally distributed slides stage. (E) Vp, density, water content and void ratio curves at the ODP 762 reveal the potential sliding surface (Hs).

ACKNOWLEDGEMENTS

We thank Geoscience Australia for providing the seismic data. The first author thanks the Shanghai Sailing Program (Grant No. 22YF1450100) and the Fundamental Research Funds for the Central Universities for their financial support.

Reference

Bull, S., Cartwright, J., and Huuse, M., 2009, A review of kinematic indicators from mass-transport complexes using 3D seismic data: Marine and Petroleum Geology, v. 26, no. 7, p. 1132-1151.

Carter, L., Milliman, J., Talling, P., Gavey, R., and Wynn, R., 2012, Near‐synchronous and delayed initiation of long run‐out submarine sediment flows from a record‐breaking river flood, offshore Taiwan: Geophysical Research Letters, v. 39, no. 12.

Clare, M. A., Talling, P. J., Challenor, P., Malgesini, G., and Hunt, J., 2014, Distal turbidites reveal a common distribution for large (> 0.1 km3) submarine landslide recurrence: Geology, v. 42, no. 3, p. 263-266.

Davies, R., Ireland, M., and Cartwright, J., 2009, Differential compaction due to the irregular topology of a diagenetic reaction boundary: a new mechanism for the formation of polygonal faults: Basin Research, v. 21, no. 3, p. 354-359.

Davies, R. J., and Clark, I. R., 2006, Submarine slope failure primed and triggered by silica and its diagenesis: Basin Research, v. 18, no. 3, p. 339-350.

Dugan, B., and Sheahan, T., 2012, Offshore sediment overpressures of passive margins: Mechanisms, measurement, and models: Reviews of Geophysics, v. 50, no. 3.

Dutkiewicz, A., Judge, A., and Müller, R. D., 2020, Environmental predictors of deep-sea polymetallic nodule occurrence in the global ocean: Geology, v. 48, no. 3, p. 293-297.

Embriaco, D., Marinaro, G., Frugoni, F., Monna, S., Etiope, G., Gasperini, L., Polonia, A., Del Bianco, F., Çağatay, M. N., and Ulgen, U. B., 2014, Monitoring of gas and seismic energy release by multiparametric benthic observatory along the North Anatolian Fault in the Sea of Marmara (NW Turkey): Geophysical Journal International, v. 196, no. 2, p. 850-866.

Foschi, M., and Cartwright, J., 2020, Seal failure assessment of a major gas field via integration of seal properties and leakage phenomena: AAPG Bulletin, v. 104, no. 8, p. 1627-1648.

Gatter, R., Clare, M., Kuhlmann, J., and Huhn, K., 2021, Characterisation of weak layers, physical controls on their global distribution and their role in submarine landslide formation: Earth-Science Reviews, v. 223, p. 103845.

Gatter, R., Clare, M. A., Hunt, J. E., Watts, M., Madhusudhan, B., Talling, P. J., and Huhn, K., 2020, A multi-disciplinary investigation of the AFEN Slide: the relationship between contourites and submarine landslides: Geological Society, London, Special Publications, v. 500, no. 1, p. 173-193.

Gay, A., Lopez, M., Cochonat, P., Séranne, M., Levaché, D., and Sermondadaz, G., 2006, Isolated seafloor pockmarks linked to BSRs, fluid chimneys, polygonal faults and stacked Oligocene–Miocene turbiditic palaeochannels in the Lower Congo Basin: Marine Geology, v. 226, no. 1-2, p. 25-40.

Haq, B., von Rad, U., and Leg, O., 1990, 122 Shipboard Scientific Party, 1990: Proc. ODP, Ink. Repts, v. 122, p. 9-15.

Kennett, J. P., Gerta Keller, M. S. Srinivasan, 1985, Miocene planktonic foraminiferal biogeography and pale-oceanographic development of the Indo-Pacific region: The Miocene Ocean: Paleoceanography and biogeography: Boulder, Colorado Geologic Society of America Memoir, p. 197-236.

L'Heureux, J.-S., Longva, O., Steiner, A., Hansen, L., Vardy, M. E., Vanneste, M., Haflidason, H., Brendryen, J., Kvalstad, T. J., and Forsberg, C. F., 2012, Identification of weak layers and their role for the stability of slopes at Finneidfjord, northern Norway, Submarine mass movements and their consequences, Springer, p. 321-330.

Locat, J., Leroueil, S., Locat, A., and Lee, H., 2014, Weak layers: their definition and classification from a geotechnical perspective, Submarine mass movements and their consequences, Springer, p. 3-12.

Masson, D., Wynn, R., and Talling, P., 2010, Large landslides on passive continental margins: processes, hypotheses and outstanding questions, Submarine mass movements and their consequences, Springer, p. 153-165.

Nähr, T., Botz, R., Bohrmann, G., and Schmidt, M., 1998, Oxygen isotopic composition of low-temperature authigenic clinoptilolite: Earth and Planetary Science Letters, v. 160, no. 3-4, p. 369-381.

Nugraha, H. D., Jackson, C. A. L., Johnson, H. D., Hodgson, D. M., and Reeve, M. T., 2018, Tectonic and oceanographic process interactions archived in Late Cretaceous to Present deep‐marine stratigraphy on the Exmouth Plateau, offshore NW Australia: Basin Research.

Paganoni, M., King, J. J., Foschi, M., Mellor-Jones, K., and Cartwright, J. A., 2019, A natural gas hydrate system on the Exmouth Plateau (NW shelf of Australia) sourced by thermogenic hydrocarbon leakage: Marine and Petroleum Geology, v. 99, p. 370-392.

Rai, A., and Singh, V., 2001, Late Neogene deep-sea benthic foraminifera at ODP Site 762B, eastern Indian Ocean: diversity trends and palaeoceanography: Palaeogeography, Palaeoclimatology, Palaeoecology, v. 173, no. 1-2, p. 1-8.

Sawyer, D. E., Flemings, P. B., Dugan, B., and Germaine, J. T., 2009, Retrogressive failures recorded in mass transport deposits in the Ursa Basin, Northern Gulf of Mexico: Journal of Geophysical Research: Solid Earth, v. 114, no. B10.

Shiwakoti, D., Tanaka, H., Tanaka, M., and Locat, J., 2002, Influences of diatom microfossils on engineering properties of soils: Soils and Foundations, v. 42, no. 3, p. 1-17.

Talling, P. J., CLARE, M. L., Urlaub, M., Pope, E., Hunt, J. E., and Watt, S. F., 2014, Large submarine landslides on continental slopes: geohazards, methane release, and climate change: Oceanography, v. 27, no. 2, p. 32-45.

Tanaka, H., and Locat, J., 1999, A microstructural investigation of Osaka Bay clay: the impact of microfossils on its mechanical behaviour: Canadian Geotechnical Journal, v. 36, no. 3, p. 493-508.

Tingay, M. R., Hillis, R. R., Swarbrick, R. E., Morley, C. K., and Damit, A. R., 2009, Origin of overpressure and pore-pressure prediction in the Baram province, Brunei: Aapg Bulletin, v. 93, no. 1, p. 51-74.

Urlaub, M., Geersen, J., Krastel, S., and Schwenk, T., 2018, Diatom ooze: Crucial for the generation of submarine mega-slides?: Geology, v. 46, no. 4, p. 331-334.

Volpi, V., Camerlenghi, A., Hillenbrand, C. D., Rebesco, M., and Ivaldi, R., 2003, Effects of biogenic silica on sediment compaction and slope stability on the Pacific margin of the Antarctic Peninsula: Basin Research, v. 15, no. 3, p. 339-363.

Figure 1

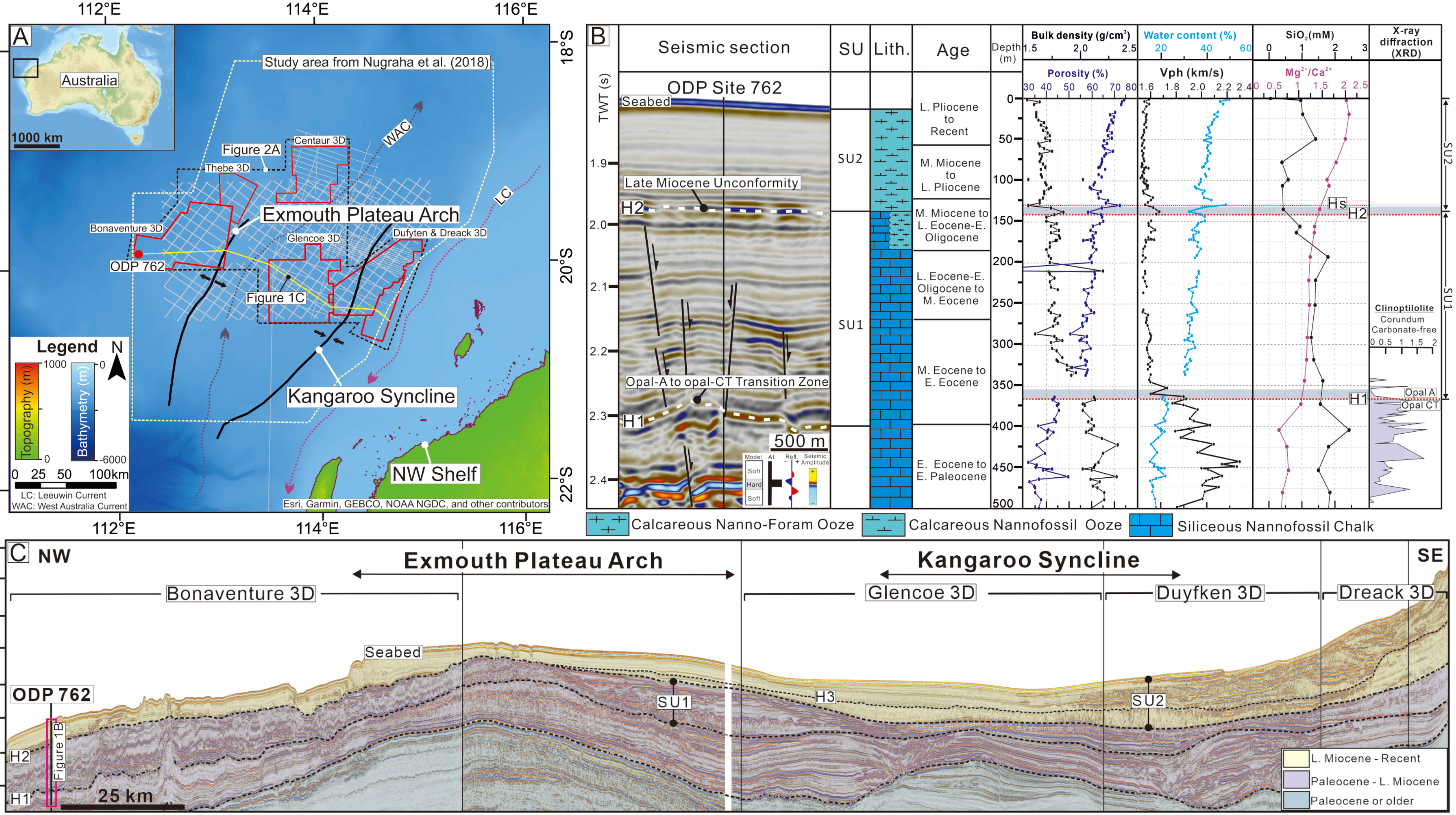

A
Australia
1000 km
Study area from Nugraha et al. (2018)
Exmouth Plateau Arch
Kangaroo Syncline
NW Shelf
ODP 762
Figure 2A
Figure 1C
Centaur 3D
Thebe 3D
Bonaventure 3D
Glencoe 3D
Dufyten & Dreack 3D
WAC
LC
Legend
Topography (m)
Bathymetry (m)
LC: Leeuwin Current
WAC: West Australia Current
Esri, Garmin, GEBCO, NOAA NGDC, and other contributors
B
Seismic section
ODP Site 762
Seabed
Late Miocene Unconformity
Opal-A to opal-CT Transition Zone
H1
H2
500 m
SU
SU1
SU2
Lith.
Age
L. Pliocene to Recent
M. Miocene to L. Pliocene
M. Miocene to L. Eocene-E. Oligocene
L. Eocene-E. Oligocene to M. Eocene
M. Eocene to E. Eocene
E. Eocene to E. Paleocene
Depth (m)
Bulk density (g/cm³)
Porosity (%)
Water content (%)
Vph (km/s)
SiO₂(mM)
Mg²⁺/Ca²⁺
X-ray diffraction (XRD)
Clinoptilolite
Corundum
Carbonate-free
Opal A
Opal CT
Hs
Calcareous Nanno-Foram Ooze
Calcareous Nannofossil Ooze
Siliceous Nannofossil Chalk
C
NW
SE
Exmouth Plateau Arch
Kangaroo Syncline
Bonaventure 3D
Glencoe 3D
Duyfken 3D
Dreack 3D
TWT (ms)
Seabed
ODP 762
Figure 1B
SU1
SU2
H3
25 km
L. Miocene - Recent
Paleocene - L. Miocene
Paleocene or older

Figure 2

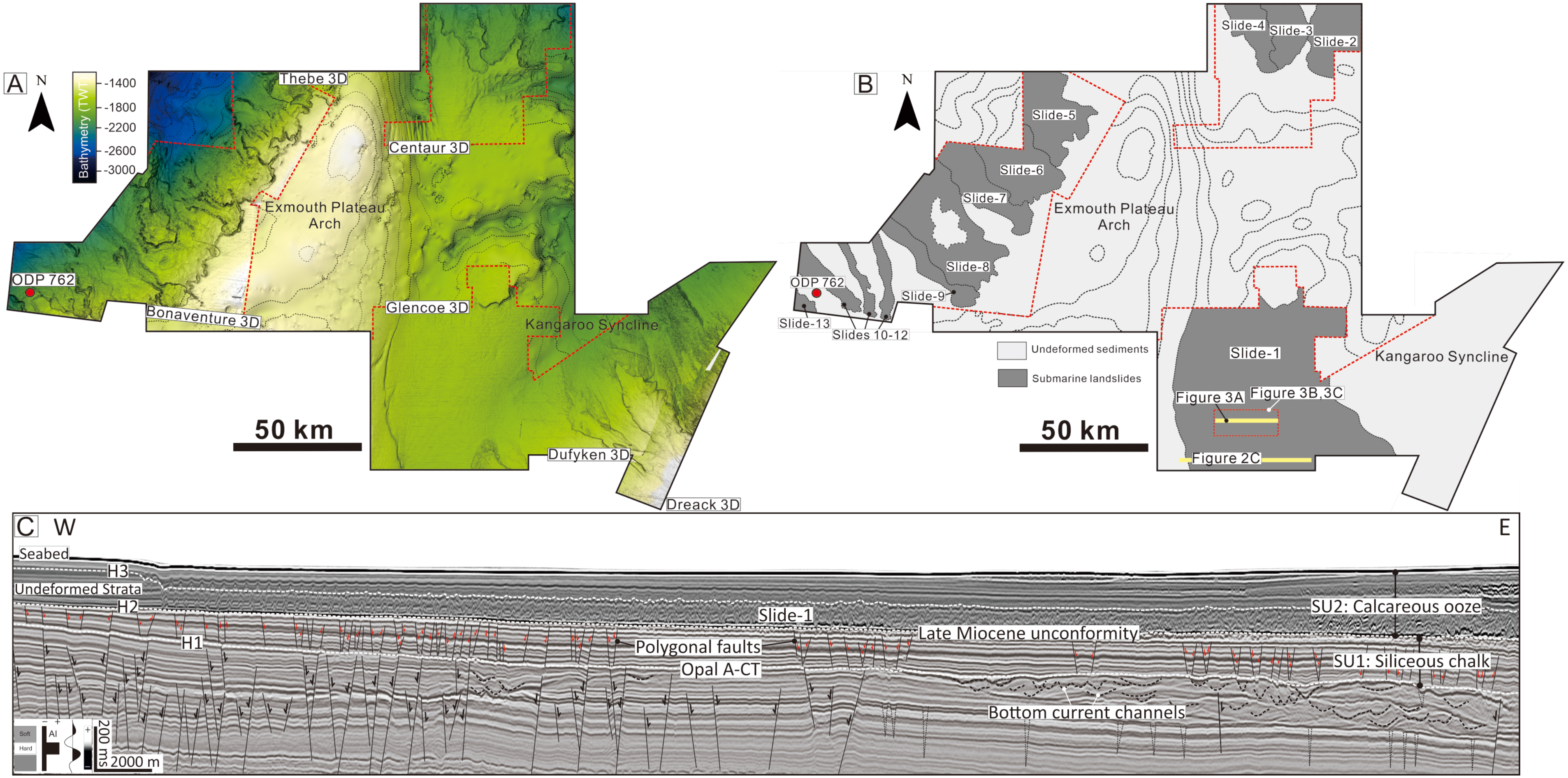
A
N
Bathymetry (TWT)
-1400
-1800
-2200
-2600
-3000
Thebe 3D
Centaur 3D
Exmouth Plateau Arch
ODP 762
Bonaventure 3D
Glencoe 3D
Kangaroo Syncline
50 km
Dufyken 3D
Dreack 3D
B
N
Slide-4
Slide-3
Slide-2
Slide-5
Slide-6
Slide-7
Exmouth Plateau Arch
Slide-8
ODP 762
Slide-9
Slide-13
Slides 10-12
Undeformed sediments
Submarine landslides
Slide-1
Kangaroo Syncline
Figure 3A
Figure 3B,3C
50 km
Figure 2C
C
W
E
Seabed
H3
Undeformed Strata
H2
H1
Slide-1
Late Miocene unconformity
Polygonal faults
Opal A-CT
SU2: Calcareous ooze
SU1: Siliceous chalk
Bottom current channels
AI
200 ms
2000 m

Figure 3

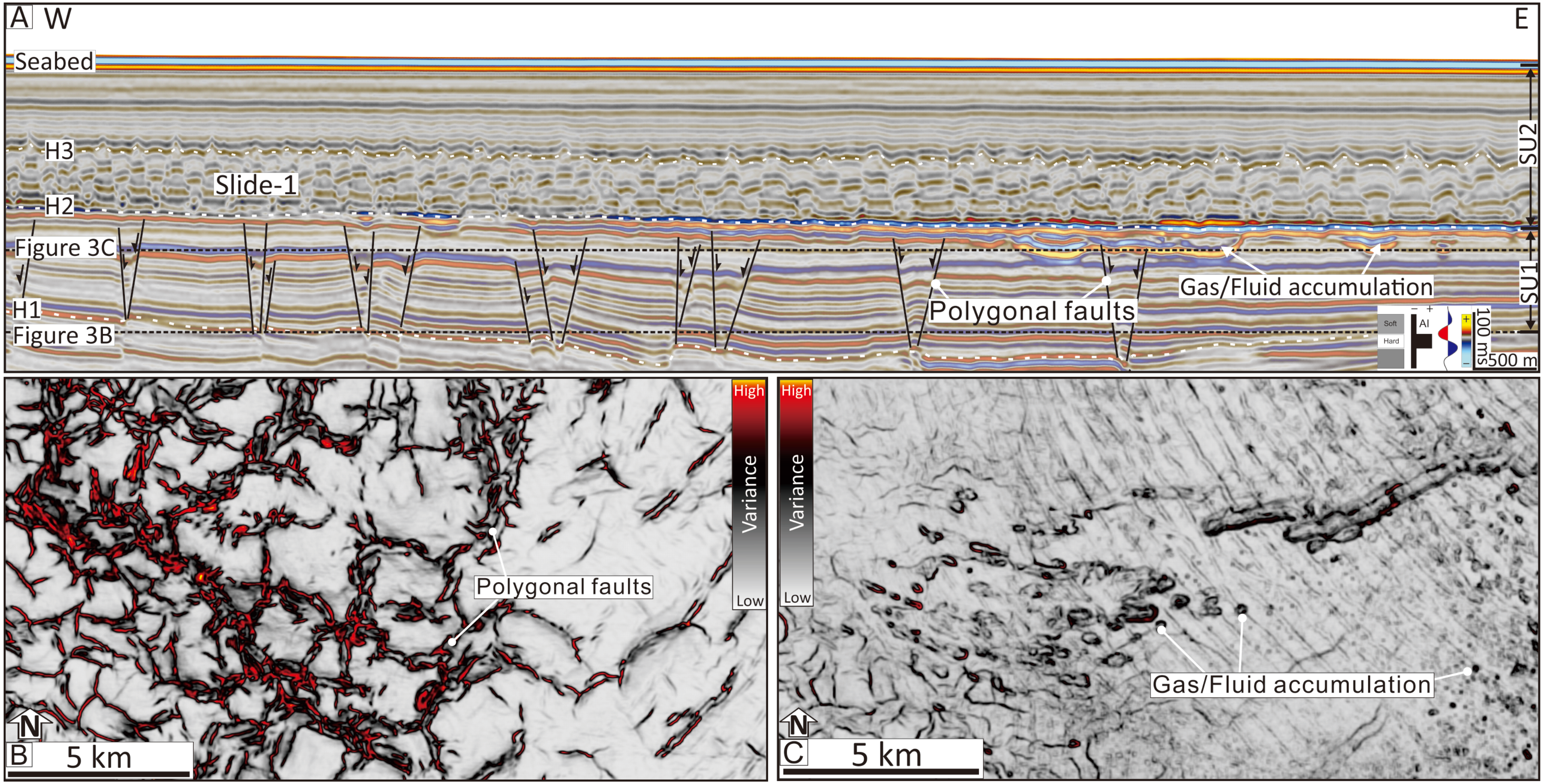

A
W
E
Seabed
H3
Slide-1
H2
Figure 3C
H1
Figure 3B
SU2
SU1
Gas/Fluid accumulation
Polygonal faults
Soft
Hard
AI
100 ms
500 m
High
Variance
Low
Polygonal faults
N
B
5 km
High
Variance
Low
Gas/Fluid accumulation
N
C
5 km

Figure 4

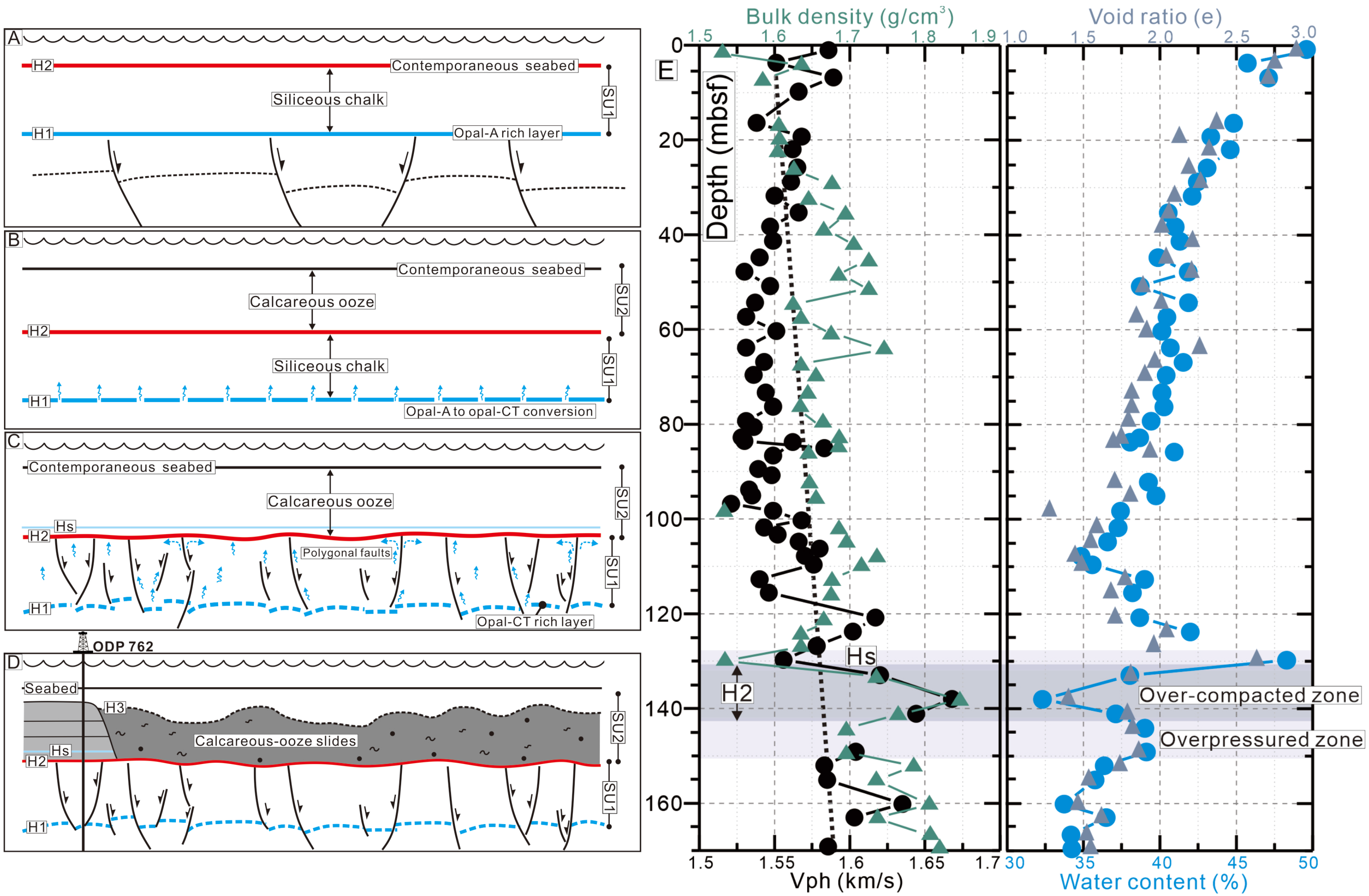

A
H2
Contemporaneous seabed
Siliceous chalk
H1
Opal-A rich layer
SU1
B
Contemporaneous seabed
Calcareous ooze
SU2
H2
Siliceous chalk
SU1
H1
Opal-A to opal-CT conversion
C
Contemporaneous seabed
Calcareous ooze
SU2
Hs
H2
Polygonal faults
SU1
H1
Opal-CT rich layer
ODP 762
D
Seabed
H3
Calcareous-ooze slides
Hs
H2
SU2
SU1
H1
E
Bulk density (g/cm³)
Void ratio (e)
Depth (mbsf)
Hs
H2
Over-compacted zone
Overpressured zone
Vph (km/s)
Water content (%)